nature communications

Article

https://doi.org/10.1038/s41467-024-54402-y

Calcium nanoparticles target and activate T cells to enhance anti-tumor function

Received: 20 February 2024

Accepted: 8 November 2024

Published online: 21 November 2024

Check for updates

Wei Yang[1], Zhizi Feng[1], Xinning Lai[1], Jianwen Li[1], Zhengwei Cao[1], Fangchao Jiang[1], Fanghui Chen[2], Shuyue Zhan[1], Feng Kong[3], Li Yang[3], Yong Teng[2], Wendy T. Watford[4], Gang Zhou[5] & Jin Xie[1]

Calcium signaling plays a crucial role in the activation of T lymphocytes. However, modulating calcium levels to control T cell activation in vivo remains a challenge. In this study, we investigate T cell activation using 12-myristate 13-acetate (PMA)-encapsulated $CaCO_3$ nanoparticles. We find that anti-PD-1 antibody-conjugated $CaCO_3$ nanoparticles can be internalized by T cells via receptor-mediated endocytosis and then gradually release calcium. This results in an increase in cytosolic calcium, which triggers the activation of NFAT and NF-κB pathways, especially when the surface of the $CaCO_3$ nanoparticles is loaded with PMA. Animal studies demonstrate that the PMA-loaded calcium nanoparticles enhance the activation and proliferation of cytotoxic T cells, leading to improved tumor suppression without additional toxicity. When tested in metastatic tumor models, T cells loaded with the calcium nanoparticles prior to adoptive cell transfer control tumor growth better, resulting in prolonged animal survival. Our approach offers an alternative T cell activation strategy to potentiate immunotherapy by targeting a fundamental signaling pathway.

T lymphocytes play a pivotal role in mediating the immunity against tumors. Central to this response are cytotoxic T lymphocytes (CTL), which have the ability to eliminate cancer cells in an antigen-specific manner[1–3]. However, tumors often create an immunosuppressive microenvironment that leads to T cell exhaustion or death, thereby undermining anti-tumor immunity[4–6]. Immune checkpoint blockade, which targets regulatory pathways to take the brakes off T cells, has achieved clinical success[7,8]. However, only a limited number of patients respond favorably to immunotherapy[9–11], highlighting the need for alternative approaches to stimulate T cell responses.

Calcium signaling is essential for T cell activation[12,13]. Upon TCR-mediated engagement with antigen-presenting cells (APC), T cells initially experience a release of calcium from the internal stores, followed by an influx of calcium through the calcium release-activated channels (CRAC)[14–16]. The increase in cytosolic calcium ($[Ca^{2+}]_i$) results in the activation of the NF-κB and NFAT pathways, leading to T cell activation[13–16]. While this physiological activation of T cells is tightly regulated by multiple signaling checkpoints, it is postulated that a chemically induced increase in $[Ca^{2+}]_i$ can directly activate T cells. This has been demonstrated with ionomycin (ION), a calcium ionophore, whose combination with 12-myristate 13-acetate (PMA) has been widely used in laboratory settings for T cell activation[17]. However, using this strategy to activate T cells in vivo has not been feasible due to the lack of selectivity and the rapid clearance of conventional ionophores.

Herein we explore a nanoparticle approach to overcome these limitations. We propose that appropriately surface-modified calcium nanoparticles can load PMA and selectively enter T cells. We hypothesize that these nanoparticles can gradually degrade inside lymphocytes, releasing both calcium and PMA into the cytosol of T cells in a controlled manner. To this end, we have successfully synthesized lipid-coated calcium carbonate nanoparticles, loaded onto the

[1]Department of Chemistry, University of Georgia, Athens, GA, USA. [2]Department of Hematology and Medical Oncology, Emory University School of Medicine, Atlanta, GA, USA. [3]Department of Plant Pathology, University of Georgia, Athens, GA, USA. [4]Department of Infectious Diseases, University of Georgia, Athens, GA, USA. [5]Georgia Cancer Center, Department of Medicine, Medical College of Georgia, Augusta, GA, USA. e-mail: gzhou@augusta.edu; jinxie@uga.edu

nanoparticles PMA, and coupled anti-PD1 antibodies onto the nanoparticle surface. Our results suggest that these nanoparticles can mimic the stimulatory effects of ION and PMA, except allowing for sustained activation of T cells, even within a complex, immunosuppressive tumor microenvironment (TME). Calcium nanoparticles are minimally toxic and readily metabolized, indicating the therapeutic and translational potential of this strategy for safely activating both endogenous and adoptively transferred T cells.

Results

Synthesis and physiochemical characterization of calcium nanoparticles

Calcium nanoparticles were synthesized according to a published protocol[18] with modifications (Fig. 1a). Transmission electron microscopy (TEM) revealed that the $CaCO_3$ nanoparticles exhibited a spherical shape with narrow size distribution (Fig. 1b) and a diameter of 110 ± 20 nm (Fig. 1c and Supplementary Fig. 1a). Energy dispersive X-ray (EDX) elemental analysis confirmed the presence of calcium, carbon, and oxygen in these nanoparticles (Fig. 1d and Supplementary Fig. 1b). X-ray diffraction (XRD) confirmed that the main composition of the nanoparticles is $CaCO_3$ (Supplementary Fig. 1c).

The calcium nanoparticles were then coated first with oleic acid (Supplementary Fig. 2a–c) and then with DSPE-PEG (1,2-distearoyl-sn-glycero-3-phosphoethanolamine-N-[carboxy(polyethylene glycol) −2000]) (Fig. 1a, Supplementary Fig. 3a). The oleic acid is bound by forming a coordinate covalent bond with surface calcium atoms, while the phospholipid is immobilized by hydrophobic-hydrophobic interaction. This two-step surface modification aims to improve the colloidal stability of the nanoparticles in water. Moreover, the coating introduces a hydrophobic interlayer that slows down the gradation of $CaCO_3$. This is important because a sustained increase of $[Ca^{2+}]_i$, rather than a transient surge, is key to chemically induced immune cell activation [19].

The oleic acid coating rendered the surface of the calcium nanoparticles less rough (Fig. 1b), but had little effect on the particle size (Fig. 1b, c, Supplementary Fig. 2a). Negative staining TEM and Fourier transform infrared spectroscopy (FT-IR) confirmed the successful oleic acid coating (Supplementary Fig. 2b, c). The surface modification is also supported by the observation that the oleic acid-coated $CaCO_3$ nanoparticles form a stable suspension in non-polar solvents (Supplementary Fig. 3b). After coating with DSPE-PEG, the nanoparticles, referred to as DCNP (both singular and plural), can be stably suspended in aqueous solutions (Supplementary Fig. 3b), with a hydrodynamic size of ~200 nm (Fig. 1f). DCNP remain stable in buffer solutions and serum, showing no significant change in size and polydispersity index (PDI) for more than 96 h (Supplementary Fig. 4a, b). Calcium release was measured in neutral pH and acidic pH solutions. At neutral pH, DCNP released ~20% of the contained calcium within the first 5 h and then reached a plateau (Fig. 1g). At pH 5.0, which is close to the pH of endosomes/lysosomes, the nanoparticles showed a controlled calcium release that lasted for more than 48 h.

We then conjugated antibodies, including those specific for CD3, CD8, PD-1, CTLA-4, and CD90.2 (Thy-1.2), to DCNP, and compared the resulting nanoconjugates for their valency (the number of antibody molecules coupled to each nanoparticle), affinity to, and uptake by T cells. These molecular targets are expressed on CTLs and, in the case of PD-1 and CTLA-4, are upregulated on tumor-infiltrating T cells[20,21]. Antibody conjugation slightly increased the hydrodynamic size of the nanoparticles (Fig. 1f) while decreasing the negativity of the surface charge (Supplementary Fig. 5). Among the antibodies tested, anti-PD-1 and anti-CD3 antibodies have relatively high valencies (Supplementary Table 1), which is expected to translate into higher binding affinity. To investigate this, we prepared Cy5-labeled and antibody-conjugated DCNP and tested them in vitro with primed OT-1 T cells. DCNP coupled with anti-PD1 or anti-CD3 antibodies are indeed associated with higher affinities to the T cells (Fig. 1h and Supplementary Fig. 6). Between the two, DCNP conjugated with anti-PD-1 antibody showed a higher degree of T cell internalization (Fig. 1i). This T cell uptake was also observed with DCNP conjugated to multiple PD-1 clones (Supplementary Fig. 7a). Furthermore, DCNP coupled to human anti-PD1 antibodies also led to internalization by human T cells (Supplementary Fig. 7b). Previous studies have shown that PD-1 can identify tumor-reactive CTLs in tumors[20,21] Considering this and the favorable uptake results, we decided to use anti-PD-1 antibody-conjugated calcium nanoparticles (referred to as DCNP-Ab) in subsequent studies.

In summary, we have successfully synthesized calcium nanoparticles and modified their surface to achieve a colloidally stable suspension. We found that calcium nanoparticles coupled with anti-PD1 antibodies can be efficiently taken up by CTLs.

Uptake of DCNP-Ab by T cells

We next investigated targeting specificity of DCNP-Ab and how they influence the $[Ca^{2+}]_i$ of T lymphocytes. We tested this at 10 μg/mL, the concentration at which DCNP-Ab showed minimal cytotoxicity (Supplementary Fig. 8). Note that DCNP-Ab at this concentration have no effect on the pH of incubation medium, even when all the nanoparticles are completely dissolved (Supplementary Fig. 4c).

Compared to DCNP not coupled with anti-PD1 antibody, DCNP-Ab showed high avidity to (Fig. 2a) and uptake by (Fig. 2b) EL4 cells, which are PD-1 positive (Supplementary Fig. 9a). DCNP-Ab showed moderate affinity to naïve OT-1 T cells (Fig. 2a). Both the avidity and cellular uptake were remarkably increased in primed T cells (Fig. 2a, b), which are high in PD-1 expression (Supplementary Fig. 9b, c). The cellular uptake of the nanoparticles was inhibited when the nanoparticles were co-incubated with dynasore, an endocytosis inhibitor of dynamin-dependent endocytosis (Fig. 2c), and less so by nystatin, which inhibits caveolae mediated cell entry[22]. In addition, the uptake was completely blocked when then temperature was lowered to 4 °C. These results suggest that DCNP-Ab target PD-1 expressed on T cells, and then enter cells through receptor-mediated endocytosis via the dynamin-dependent pathway.

We next investigated the selectivity of the nanoparticles by incubating dye-labeled DCNP-Ab with splenocytes from OT-1 mice, which contain T lymphocytes as well as myeloid cells such as macrophages. In unstimulated splenocytes, the uptake of DCNP-Ab by CTLs was comparable to that in myeloid cells (Fig. 2d). The difference was significantly increased when the splenocytes were incubated with OVA peptide, which induced PD-1 expression on CTLs (Supplementary Fig. 10a), resulting in a preferential uptake of DCNP-Ab by CTLs. We also tested DCNP-Ab with splenocytes from wild-type C57BL/6 mice, in which the T cell population is not skewed toward $CD8^+$ T cells. DCNP-Ab showed favorable uptake by $PD\text{-}1^+$ cells (Fig. 2e), the majority of which are lymphocytes. More DCNP-Ab were found in $CD8^+$ than in $CD4^+$ T cells, likely due to the relatively high PD-1 levels among activated CTLs (Supplementary Fig. 11). Interestingly, within the $CD4^+$ T cells, the majority of the nanoparticles were found in Th1 cells rather than in Th2 cells, and few DCNP-Ab were found in Tregs (Fig. 2e).

We then examined the influence of DCNP-Ab on cytosolic calcium levels using Fluo-3 AM as an indicator of $[Ca^{2+}]_i$. When tested in EL4 cells, DCNP-Ab caused a significant increase in $[Ca^{2+}]_i$ that persisted for more than 24 h (Fig. 2f). In comparison, calcium salts such as $CaCl_2$ had no effect on $[Ca^{2+}]_i$ (Fig. 2f). Incubation with DCNP-Ab also significantly increased $[Ca^{2+}]_i$ in primed OT-1 T cells (Fig. 2g) and human T cells (Supplementary Fig. 12). In addition, we tested DCNP conjugated with antibodies specific for CD3, CD8, PD-1, CTLA-4, and CD90.2. Consistent with the nanoparticle uptake results (Fig. 1i), these conjugates either showed no effect on $[Ca^{2+}]_i$ or were less effective at elevating $[Ca^{2+}]_i$ (Fig. 2h).

Taken together, our results suggest that DCNP-Ab can be selectively taken up by T cells through PD-1-mediated endocytosis, and

https://doi.org/10.1038/s41467-024-54402-y

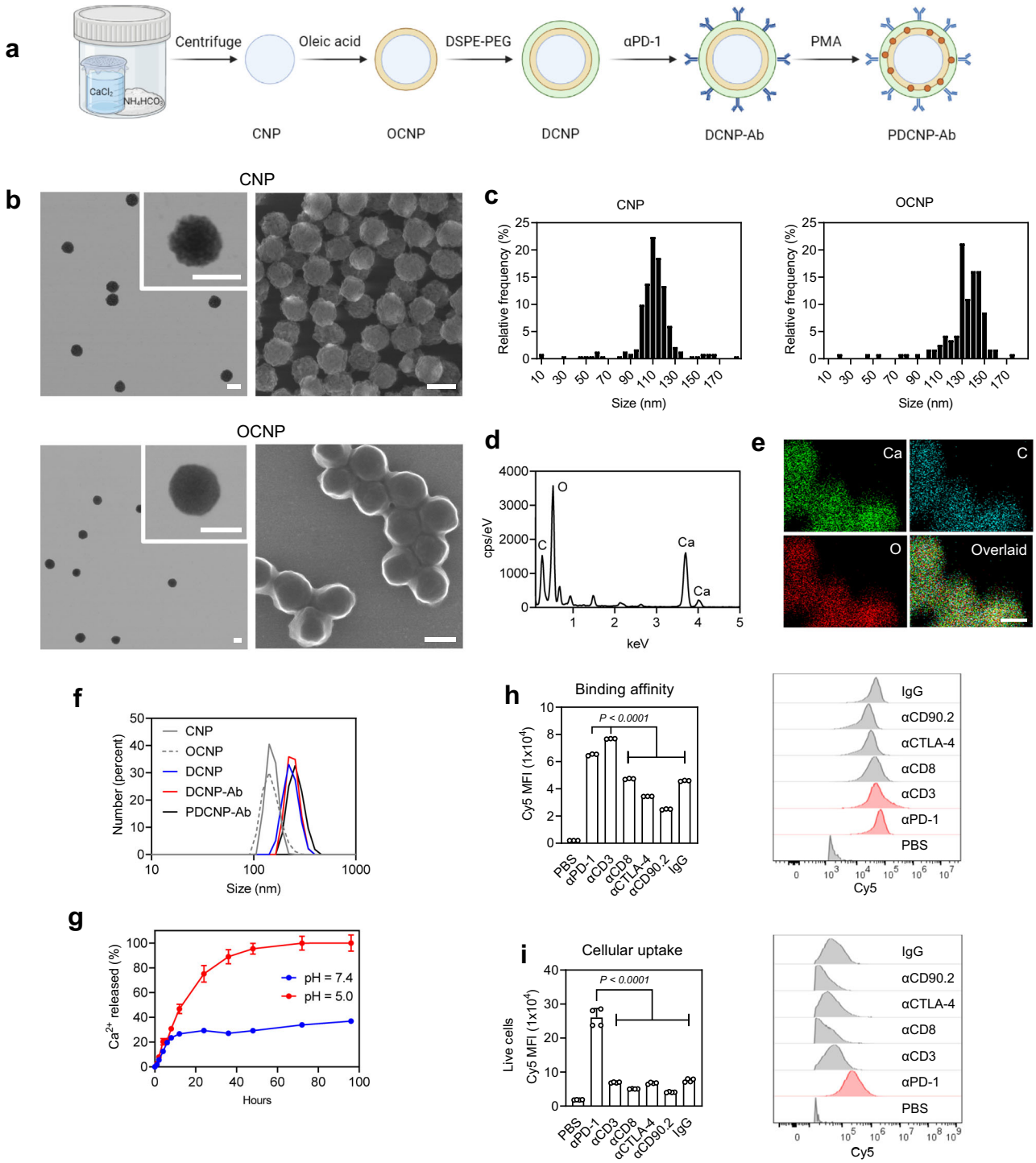

Fig. 1 | Synthesis of antibody-conjugated calcium nanoparticles. a Schematic diagram of nanoparticle synthesis. $CaCO_3$ nanoparticles were first coated with oleic acid and then with DSPE-PEG-COOH. The resulting, lipid-coated calcium nanoparticles were conjugated with anti-PD1 antibody and then loaded with PMA. CNP, $CaCO_3$ nanoparticles; OCNP, oleic acid-coated CNP; DCNP, DSPE-PEG-coated OCNP; DCNP-Ab, αPD-1-conjugated DCNP; PDCNP-Ab, PMA-loaded DCNP-Ab. Created in BioRender. Li, J. (2024) https://BioRender.com/h52j842. **b** Representative TEM (left) and SEM (right) images of CNP and OCNP. The experiment was repeated independently at least three times with similar results. Insets: zoom-in TEM images of a single CNP or OCNP. Scale bars, 100 nm. **c** Size distribution of CNP (left) and OCNP (right), analyzed by ImageJ based on TEM images. The average nanoparticle sizes are 110 and 135 nm, respectively, for CNP and OCNP. **d** EDX spectrum of CNP. The experiment was repeated independently at least three times with similar results. **e** EDX elemental mapping images of CNP. Green, calcium; blue, carbon; red, oxygen. The experiment was repeated independently at least three times with similar results. Scale bar, 50 nm. **f** Hydrodynamic sizes of CNP, OCNP, DCNP, DCNP-Ab, and PDCNP-Ab, measured by DLS. The experiment was repeated independently three times with similar results. **g** Calcium release profiles of DCNP-Ab, measured in solutions of neutral (pH 7.4) and acidic (pH 5.0) pH (n = 3 independent experiments). Binding affinity (**h**) and cellular uptake (**i**) of antibody-conjugated DCNP, assessed with fixed and live OT-1 CTLs, respectively (n = 3 biologically independent samples for (**h**), and n = 4 biologically independent samples for (**i**). DCNP were conjugated with antibodies specific to PD1, CD3, CD8, CTLA-4, or CD90.2 or mouse IgG and were labeled with Cy5. Left, bar graphs comparing the MFI of Cy5 in cells. Right, histograms showing the distribution of Cy5 fluorescence intensity. Data represent mean ± SD. Statistical difference was evaluated using a one-way ANOVA test. Source data underlying (**c**, **d**) and (**f**–**i**) are provided in a Source Data file.

https://doi.org/10.1038/s41467-024-54402-y

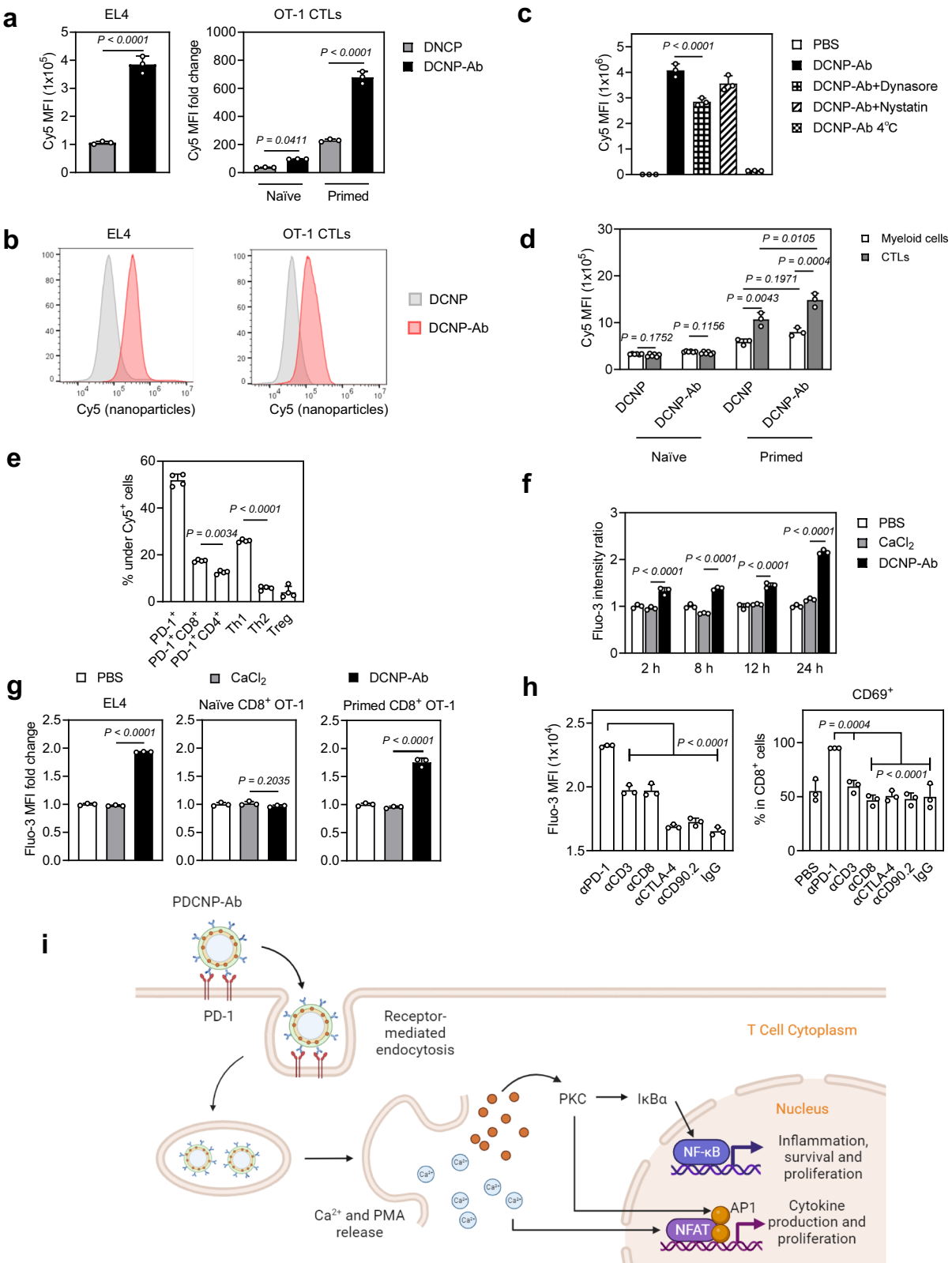

gradually degraded inside the cells to release calcium, resulting in a sustained increase in $[Ca^{2+}]_i$ (Fig. 2i).

Influence on the functions of T cells

We reasoned that by increasing $[Ca^{2+}]_i$, DCNP-Ab, similar to calcium ionophores such as ION, may activate the NF-κB and NFAT signaling pathways (Fig. 2i). This was confirmed by Western blot, which showed increased phosphorylation of NF-κB and the dephosphorylation of NFAT in T lymphocytes treated with DCNP-Ab (Fig. 3a, b). This leads to the activation of T cells, manifested by an increased expression of CD69 (Fig. 2h). Note that calcium nanoparticles conjugated with anti-CD3, -CD8, -CTLA4, -CD90.2 antibodies and IgG showed little or no effect on T cell stimulation (Fig. 2h).

Fig. 2 | Uptake of antibody-conjugated calcium nanoparticles by T lymphocytes. a Binding affinity of DCNP-Ab (Cy5-labeled) to fixed EL4 cells and OT-1 CTLs (naïve or primed). Cy5-labeled DCNP were tested for comparison (n = 3 biologically independent samples). **b** Cellular uptake of DCNP-Ab or DCNP by EL4 and primed $CD8^+$ OT-1 T cells, repeated three times independently with similar results. **c** Endocytosis of DCNP-Ab (Cy5-labeled), assessed with EL4 cells (n = 3 biologically independent samples). **d** Uptake of Cy5-labeled DCNP or DCNP-Ab by splenocytes from OT-1 mice. Uptake by myeloid cells ($CD11b^+$) and CTLs ($CD8^+$) were analyzed by flow cytometry (n = 6 biologically independent samples for the naïve group and 3 for the primed group). **e** Uptake of Cy5 labeled DCNP-Ab by splenocytes from normal C57/BL6 mice (n = 4 biologically independent samples). Th1, $CD4^+$T-bet^+; Th2, $CD4^+GATA3^+$; Tregs, $CD4^+Foxp3^+CD25^+$. **f** Changes in $[Ca^{2+}]_i$, measured with Fluo-3 AM in EL4 cells. $CaCl_2$ and PBS were tested for comparison (n = 3 biologically independent samples). **g**, $[Ca^{2+}]_i$ change after incubation with DCNP-Ab, evaluated in EL4 cells, naïve OT-1 CTLs, and primed OT-1 CTLs. $CaCl_2$ salt and carrier only (PBS) were tested for comparison (n = 3 biologically independent samples). **h** T cell $[Ca^{2+}]_i$ (left) and activation (right) after incubation with nanoconjugates, evaluated with enriched $CD8^+$ OT-1 T cells (n = 3 biologically independent samples). Nanoconjugates include those formed between DCNP and αPD-L1 (i.e., DCNP-Ab), αCD3, αCD8, αCLTA4, αCD90.2, and IgG antibodies. Flow cytometry was used to measure Fluo-3 MFI (left) and $CD69^+$ expression (right) after 24 h of incubation. **i** Schematic illustration of T cell activation by PDCNP-Ab. PDCNP-Ab are taken up by T cells through endocytosis by engaging surface PD-1. The nanoparticles release Ca^{2+} and PMA inside the cells, resulting in the activation of the NFAT and NF-κB pathways, culminating in T cell activation. Created in BioRender. Li, J. (2024) https://BioRender.com/u22v821. Data represented mean ± SD. Statistical difference was evaluated using a one-way ANOVA test in (**a**) (OT-1 CTLs), (**c**–**h**), and unpaired Student's t-test (one-tailed) in (**a**) (EL4). Source data underlying (**a**–**h**) are provided in a Source Data file.

As mentioned above, PMA, a PKC activator, is often used in the laboratory setting in combination with ION to activate T cells[23]. Inspired by this, we loaded PMA onto DCNP-Ab for co-delivery of calcium and PMA. As a diacylglycerol analog with a long alkyl chain, PMA is efficiently loaded onto DCNP-Ab by insertion into the lipid coating layer. High-performance liquid chromatography (HPLC) analysis showed that the loading capacity of PMA can be up to 8% (Supplementary Fig. 13). We typically used a formulation with a weight ratio of PMA to calcium of 1:20 (corresponding to a loading capacity of 1%). The resulting PMA-loaded nanoparticles, termed PDCNP-Ab, showed comparable hydrodynamic size (Fig. 1f) and surface zeta potential (Supplementary Fig. 5) to DCNP-Ab. The PMA loading also has a negligible effect on nanoparticle avidity and cytotoxicity (Supplementary Fig. 8).

Compared to DCNP-Ab, PDCNP-Ab was more effective in activating the NF-κB and NFAT pathways, as confirmed by Western blotting in both enriched OT-1 T cells and EL4 cells (Fig. 3a, b). Impressively, PDCNP-Ab were more potent than ION/PMA in activating the two pathways. The superior stimulatory effect was attributed to the ability of PDCNP-Ab to deliver synergistic calcium and PMA signals into lymphocytes.

Next, we investigated the effect of PDCNP-Ab on T lymphocyte functions. We studied this in naïve and peptide-primed OT-1 splenocytes, using ION/PMA and $CaCl_2$ as controls. ION/PMA similarly activated lymphocytes, evidenced by increased expression of CD69, IFN-γ, and TNF-α in both naïve and primed T cells (Fig. 3c). PDCNP-Ab exhibited comparable or superior stimulatory effects to ION/PMA in primed T cells (Fig. 3c); meanwhile, their effect on naïve T cells was modest, likely due to the differential expression of PD-1 on these cells (Fig. 3d). Additionally, we found that PDCNP-Ab induced a more pronounced increase in CD69, IFN-γ, and TNF-α among $PD\text{-}1^+$ cells compared to $PD\text{-}1^-$ CTLs (Supplementary Fig. 14), further supporting the PD-1 targeted delivery of the nanoparticles.

Effective T cell activation was further validated by analyzing cytokine secretion. Consistent with the flow cytometry results, PDCNP-Ab effectively induced the secretion of IL-2, IFN-γ, and TNF-α in primed T cells (Fig. 3f and Supplementary Fig. 15). Moreover, PDCNP-Ab resulted in higher secretion levels of IFN-γ and TNF-α compared to ION/PMA, especially at later time points (Supplementary Fig. 15). Interestingly, IL-2 levels declined more rapidly in primed T cells treated with PDCNP-Ab than with ION/PMA (Supplementary Fig. 15). This is likely due to the consumption of IL-2 by activated T cells[24,25], which is more strongly induced by PDCNP-Ab.

To further validate our findings, we tested the nanoparticles in OT-1 T cells primed with αCD3/αCD28 (Fig. 3g), OT-1 T cells co-cultured with pre-irradiated B16F10-OVA cells (Supplementary Fig. 16), and EL4 cells (Fig. 3h). We observed similar stimulation with PDCNP-Ab, and the stimulatory effects lasted longer than with ION/PMA (Fig. 3g). Notably, anti-PD1 antibody alone, at equivalent or 10-fold concentrations, had no effect on T cell stimulation (Fig. 3h). Degraded PDCNP-Ab (by dissolving the $CaCO_3$ core in mild acidic solutions), which lost the ability to cross the cell membrane, also failed to activate T cells (Fig. 3h).

Furthermore, we tested PDCNP-Ab ex vivo with splenocytes harvested from healthy C57BL/6 mice. ION/PMA promoted the expansion of both $CD8^+$ and $CD4^+$ T lymphocytes, including Tregs (Supplementary Fig. 17a). In comparison, PDCNP-Ab had a more pronounced effect on CTLs, consistent with the $[Ca^{2+}]_i$ data. We also tested PDCNP-Ab with splenocytes taken from tumor-bearing mice that had undergone unsuccessful αPD-1 immunotherapy. Increased levels of Tregs in the secondary lymphoid organs are commonly seen in tumor-bearing mice and negatively correlate with response to immunotherapy[26,27]. Indeed, we observed a much higher level of Tregs and a lower frequency of CTLs in splenocytes from these animals (Supplementary 17b). Incubation with PDCNP-Ab significantly increased the percentage of T lymphocytes, especially CTLs, in the splenocytes (Supplementary Fig. 17c). Notably, the ratio of effector CTLs to Treg cells was significantly increased after nanoparticle treatment, suggesting the ability of PDCNP-Ab to activate or reinvigorate T lymphocytes.

In summary, our results demonstrate that PDCNP-Ab can effectively stimulate T cells by activating the NF-κB and NFAT pathways. Unlike ION/PMA, which indiscriminately stimulates all lymphocytes, the stimulatory effects of PDCNP-Ab are more focused on $PD\text{-}1^+$ CTLs.

Influence of PDCNP-Ab on the TME

We then evaluated the tumor retention of intratumorally (i.t.) administered, dye-labeled PDCNP-Ab. Whole-body fluorescence imaging revealed that, compared to nanoparticles not conjugated with anti-PD1 antibodies, PDCNP-Ab remained in tumors longer after injection (Supplementary Fig. 18a–d). This was further supported by microscopic analysis, which found more PDCNP-Ab in tumors after 24 h, many of which were within $PD1^+$ CTLs (Supplementary Figs. 19, 20). Flow cytometry showed that both $CD4^+$ and $CD8^+$ T cells in these tumors were predominantly PD-1 positive, and PDCNP-Ab were preferentially taken up by the T cells compared to phagocytes, including macrophages and dendritic cells, and B cells (Supplementary Fig. 21).

The influence of intratumoral PDCNP-Ab on the TME was then evaluated in B16F10-OVA tumor-bearing mice (Fig. 4a). Injection of PDCNP-Ab (125 μg/kg, three doses for every three days, i.t.) significantly increased the levels of tumor-infiltrating CTLs and effector CTLs (Fig. 4b), while reducing the population of Tregs ($p = 0.1405$, Fig. 4b). Additionally, a significantly increased frequency of $Ki67^+$ cells was found among both tumor-infiltrating CTLs (Fig. 4b) and CTLs in the tumor-draining lymph node (TDLN, Supplementary Fig. 22), indicating enhanced CTL expansion. Notably, DCNP-Ab also led to increased CTL/Treg ratios in tumors (Fig. 4b), though it was not as effective as PDCNP-Ab. Unlike in vitro studies, intratumoral ION/PMA showed little effect on CTL infiltration and activation in tumors, likely

https://doi.org/10.1038/s41467-024-54402-y

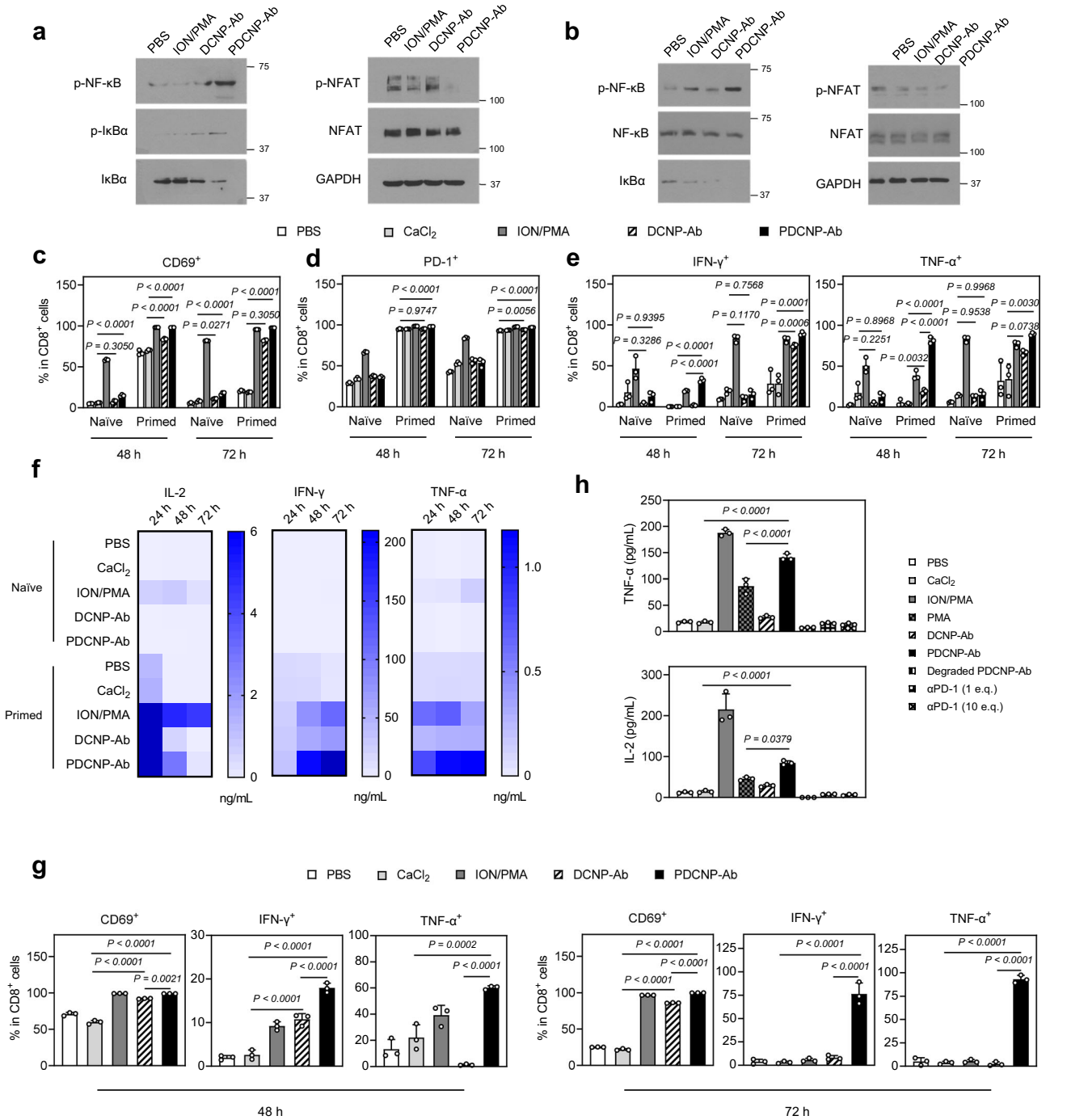

Fig. 3 | Influence of antibody-conjugated calcium nanoparticles on T-cell activation. Cells were incubated with PDCNP-Ab (10 μg·Ca/mL, loaded with 0.5 wt% PMA, equivalent to 50 ng/mL) or an equivalent amount of DCNP-Ab. For comparison, ION/PMA (1.34 μM/50 ng/mL) or PBS were tested. Western blotting analysis of NF-κB and NFAT pathway activation in (**a**) enriched OT-1 CTLs and (**b**) EL4 cells. The experiment was repeated three times independently with similar results. T cell activation was assessed by flow cytometry, which examined the frequencies of $CD69^+$ (**c**), $PD\text{-}1^+$ (**d**), and $IFN\text{-}\gamma^+$ or $TNF\text{-}\alpha^+$ (**e**) cells within the $CD8^+$ cell population. The study was performed with splenocytes from OT-1 mice, which were either untreated or primed with SIINFEKL peptide (n = 3 biologically independent samples). **f** Release of IL-2, IFN-γ, and TNF-α at 24, 48, and 72 h, measured by ELISA (n = 3 biologically independent samples). The study was performed with splenocytes from OT-1 mice, with or without stimulation with SIINFEKL peptide. **g** T cell activation, assessed with OT-1 splenocytes activated with αCD3/αCD28 at 48 or 72 h of incubation (n = 3 biologically independent samples). **h** Influence of PDCNP-Ab on the secretion of IL-2 and TNF-α, tested with EL4 cells. Controls included αPD-1 antibody alone at 1 × (1 e.q.) or 10 × (10 e.q.) equivalent doses, as well as degraded PDCNP-Ab (n = 3 biologically independent samples). Data represent mean ± SD. Statistical difference was evaluated by one-way ANOVA in (**c**–**e**), (**h**), (**g**). Source data underlying (**c**–**g**) are provided in a Source Data file.

due to its rapid clearance and therefore inefficiency in maintaining a meaningful stimulatory effect.

We also co-cultured splenocytes from the treated animals with B16F10-OVA cancer cells ex vivo. Samples from the PDCNP-Ab group showed enhanced T cell proliferation (Fig. 4c) and an increased expansion of tumor-reactive T cells (Fig. 4d) over the incubation. In contrast, splenocytes from the ION/PMA group showed no difference in T cell expansion and activation compared to those from the carrier-only control. These results again support that PDCNP-Ab, but not ION/PMA, have the ability to expand tumor-reactive T cells in vivo.

https://doi.org/10.1038/s41467-024-54402-y

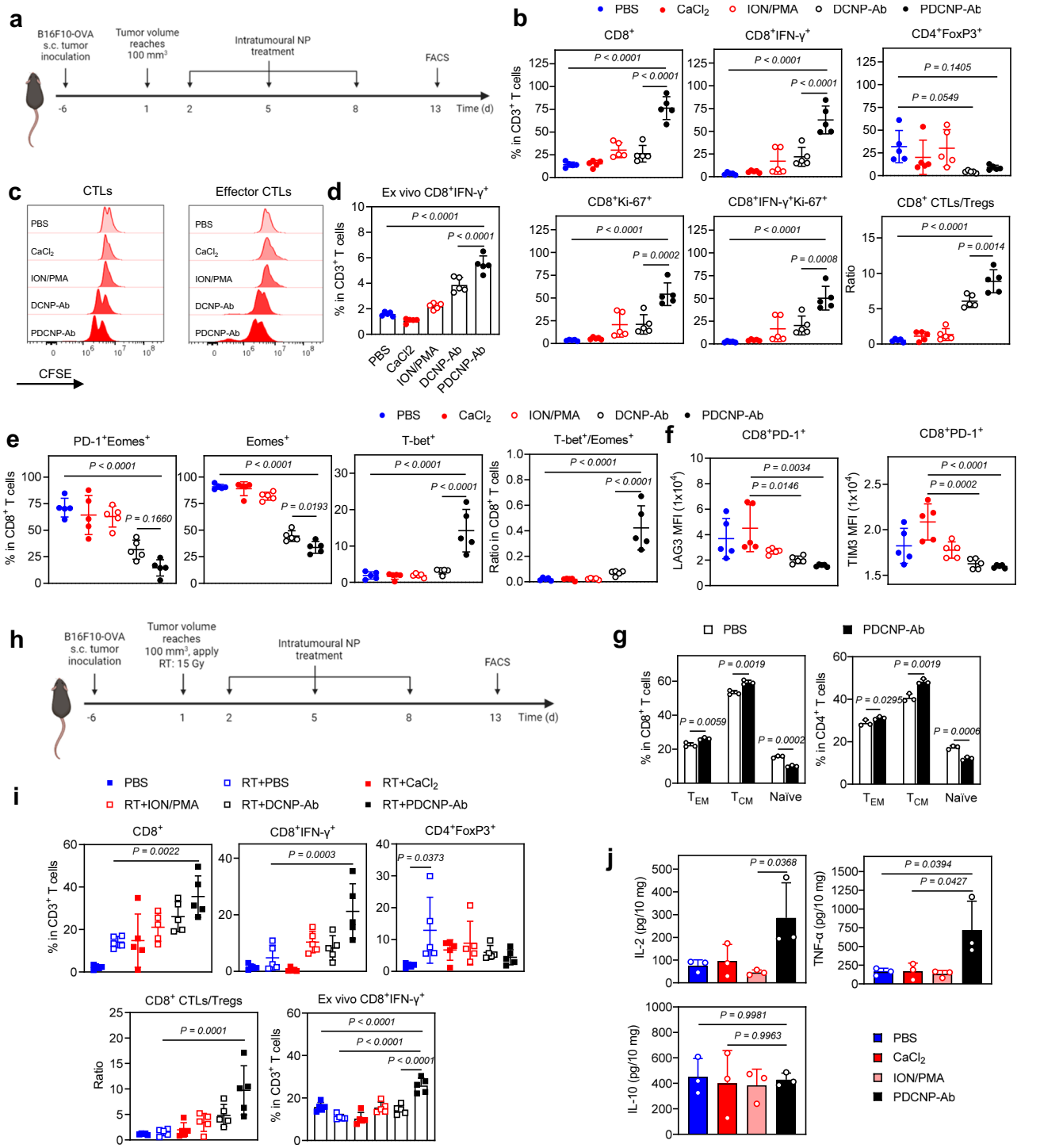

Fig. 4 | Impact of PDCNP-Ab on the TME. PDCNP-Ab (125 μg·Ca/kg, loaded with 0.5 wt% PMA) were administered i.t. For comparison, equivalent doses of DCNP-Ab, calcium salt, ION/PMA (6.7 nM/kg and 250 ng/kg, respectively), and PBS were injected. **a** Timeline of nanoparticle injections and flow cytometry analysis; experiments were conducted in B16F10-OVA tumor-bearing mice. Created in BioRender. Li, J. (2024) https://BioRender.com/i82v387. **b** Profiles of tumor-infiltrating T cells, including T cells ($CD3^+CD8^+$), effector T cells ($CD3^+CD8^+IFN\gamma^+$), proliferating T cells ($CD3^+CD8^+Ki67^+$), and Tregs ($CD3^+CD4^+FoxP3^+$) (n = 5 mice). T cell expansion (**c**) and activation (**d**), investigated ex vivo by co-culturing splenocytes isolated from different treatment groups with B16F10-OVA cells (n = 5 mice). Influence on T cell exhaustion. **e** Frequencies of $Eomes^+$, $PD1^+Eomes^+$, and $T\text{-}bet^+$ cells in CTLs as well as $T\text{-}bet^+/Eomes^+$ ratios among CTLs (n = 5 mice). **f** MFI of LAG3 and TIM3 in $PD\text{-}1^+$ CTLs (n = 5 mice). The experimental scheme is shown in Supplementary Fig. 24a. **g** Changes of naïve, T_{CM}, and T_{EM} populations among spleen CTLs, measured one week after treatment with PDCNP-Ab or PBS (n = 3 biologically independent samples). **h** Therapeutic treatment regimen. The experiments were conducted in B16F10-OVA tumor-bearing mice. Irradiation (RT) was applied to tumors on Day 1. PDCNP-Ab and controls were administered i.t. on Day 2, 5, and 8. Animals were euthanized on Day 13 for flow cytometry analysis. Created in BioRender. Li, J. (2024) https://BioRender.com/m87w815. **i** Profiles of tumor-infiltrating T cells, including T cells ($CD3^+CD8^+$), effector T cells ($CD3^+CD8^+IFN\gamma^+$), and Tregs ($CD3^+CD4^+FoxP3^+$). In addition, splenocytes from the treatment groups were co-cultured ex vivo with B16F10-OVA cells (n = 5 mice). **j** Levels of cytokines, including IL-2, TNF-α, and IL-10, in tumor tissues, analyzed by ELISA (n = 3 biologically independent samples). Data represent mean ± SD. Statistical difference was evaluated using an unpaired Student's t-test (one-tailed) in (**g**), and a one-way ANOVA test in (**b**, **d**–**f**, **i**, **j**). Source data underlying (**b**–**f**) and (**g**–**j**) are provided in a Source Data file.

Importantly, treatment with PDCNP-Ab also resulted in reduced levels of exhausted T cells in tumors. This is evidenced by decreased percentages of Eomes$^+$ cells in tumors treated with the nanoparticles (Fig. 4e). This change was accompanied by an increased frequency of T-bet$^+$ CTLs, and a higher T-bet$^+$/Eomes$^+$ ratio among CTLs (Fig. 4e and Supplementary Fig. 23). Moreover, unlike calcium salt, which had no effect on the expression of LAG-3 or TIM-3, PDCNP-Ab significantly reduced the expression of these exhaustion markers in tumor CTLs (Fig. 4f). These observations suggest that PDCNP-Ab can reinvigorate exhausted T cells[28], which in the absence of treatment expand as tumors grow (Supplementary Fig. 24b). Furthermore, flow cytometry revealed a shift of splenic lymphocytes from naïve T cells to central memory T cells (T_{CM}) in both the CD8$^+$ and CD4$^+$ populations in animals treated with PDCNP-Ab (Fig. 4g), indicating that the treatment also induced long-term immune memory in these animals.

Next, we tested the effect of PDCNP-Ab on irradiated tumors (Fig. 4h). There is an increased uptake of PDCNP-Ab by lymphocytes (Supplementary Fig. 21), possibly due to radiation-induced expression of PD-1[29]. While irradiation facilitated the tumor infiltration of CTLs, it did not increase the number of effector CTLs but instead enhanced the recruitment of Tregs (Fig. 4i). Treatment with PDCNP-Ab resulted in an increased frequency of effector CTLs and higher CTL/Treg ratios in tumors (Fig. 4i). The stimulatory effect was also demonstrated by elevated levels of IL-2 and TNF-α in tumors (Fig. 4j), increased proliferation of CTLs in TDLN (Supplementary Fig. 25), and a higher frequency of effector CTLs among splenocytes when co-cultured ex vivo with B16F10-OVA cancer cells (Fig. 4i).

Collectively, our results demonstrate that intratumoral PDCNP-Ab can activate and/or reinvigorate T cells, thereby altering the TME. The treatment led to the expansion of tumor-reactive T cells, which translates into an enhanced cellular immune response.

Therapeutic benefits of PDCNP-Ab

Next, we evaluated the therapeutic benefit of PDCNP-Ab in B16F10 tumor-bearing C57BL/6 mice. A total of three doses of PDCNP-Ab (125 μg/kg) were administered i.t. three days apart (Fig. 5a). PDCNP-Ab significantly improved tumor suppression and animal survival (Fig. 5b, Supplementary Fig. 26). Post-mortem immunohistochemistry revealed a significant increase in T lymphocyte infiltration, accompanied by a marked decrease in Ki-67 and CD31-positive cells (Fig. 5c). In contrast, depletion of CTLs with anti-CD8 antibodies almost completely abolished the therapeutic benefit of PDCNP-Ab (Fig. 5b, Supplementary Fig. 26) and reversed the inhibition of cancer cell proliferation and angiogenesis (Fig. 5c). This indicates that tumor suppression with PDCNP-Ab was largely mediated by CTLs. For validation, we also tested PDCNP-Ab in MB49 tumor-bearing mice and observed a similar degree of tumor suppression, which was attenuated when the animals were pre-treated with anti-CD8 antibodies (Fig. 5d, Supplementary Fig. 27, 28). Importantly, no decrease in body weight or signs of acute or long-term toxicity were observed in animals treated with PDCNP-Ab.

To further evaluate potential side effects, we performed a complete blood count (CBC) and histopathology on PDCNP-Ab-treated animals. This was studied in B16F10 tumor-bearing mice with i.t. injected PDCNP-Ab, and in healthy mice, where the nanoparticles were injected subcutaneously (s.c.) into the flanks. The CBC detected no abnormalities beyond tumor-associated aberrations (Fig. 5e). Despite the enhanced intratumoral immune response induced by PDCNP-Ab, we did not observe any signs of inflammation or toxicity in the major organs (Supplementary Fig. 29). In addition, there was no significant increase in serum calcium levels (Fig. 5f), which is not surprising given the small injection dose. Altogether, these results suggest that PDCNP-Ab was well tolerated by the animals.

Subsequently, we evaluated the efficacy of PDCNP-Ab when used in combination with radiation therapy (RT). Briefly, B16F10 tumors received three fractions of 5 Gy radiation at three-day intervals on Day 1, 4, and 7. Nanoparticles were administered i.t. one day after each radiation treatment (Fig. 5g). B16F10 tumors are known to be resistant to radiation[30], and all animals in the RT-only group experienced rapid tumor relapse by week 3, and reached a humane endpoint by week 4 (Fig. 5h). $CaCl_2$ salt had no effect on tumor growth. In contrast, all animals treated with PDCNP-Ab in addition to radiation remained tumor-free on day 25 (Fig. 5h). Median survival was significantly prolonged to 45 days, compared to 27 days with RT alone.

In conclusion, our results suggest that PDCNP-Ab, by activating T cells and altering the TME, can be used as a stand-alone treatment or in combination with conventional therapies such as radiation to improve tumor suppression without causing additional systemic toxicity.

Adoptive cell therapy with PDCNP-Ab loaded lymphocytes

We hypothesize that PDCNP-Ab can be loaded into T lymphocytes ex vivo to maintain their activation status in vivo, thereby enhancing the efficacy of adoptive cell therapy. We first tested this with OT-1 T cells. Compared to conventional stimulatory protocol[31], pre-incubation with PDCNP-Ab significantly increased the expression of CD69, TNF-α, and IFN-γ in lymphocytes, indicating their conversion to effector T cells (Fig. 6a). In addition, we observed a shift in the cell population from naive T cells to T_{CM} and effector memory T cells (T_{EM}). The percentages of proliferating T_{CM} and T_{EM} cells also increased significantly (Fig. 6b and Supplementary Fig. 30), which are favorable factors for a durable immune response in vivo [32].

To evaluate efficacy, we administered OT-1 T cells, stimulated ex vivo with either a conventional protocol or with PDCNP-Ab, into B16F10-OVA tumor-bearing mice. Lymphodepletion with whole-body irradiation, except for the tumor area, was performed prior to the adoptive cell transfer (Fig. 6c). Intravenous OT-1 T cells significantly prolonged the survival of the animals, with 20% of the mice remaining tumor-free on Day 60 (Fig. 6d). Compared to T cells stimulated by a conventional method, those loaded with PDCNP-Ab prior to administration resulted in significantly improved tumor suppression and animal survival. Impressively, 80% of the mice in the PDCNP-Ab group experienced complete tumor regression (Fig. 6d, Supplementary Fig. 31). All of the surviving animals also successfully rejected a rechallenge with live B16F10-OVA cells inoculated on Day 60.

Finally, we tested adoptive cell transfer with T lymphocytes isolated from PMEL-1 mice. PMEL-1 T cells recognize gp100, a common tumor-associated antigen in many cancer cells, including B16F10. We evaluated the efficacy in a metastatic tumor model established by i.v. injection of B16F10-fLuc cells. After 7 days, the animals received intravenous administration of PMEL-1 T cells stimulated with PDCNP-Ab or by a conventional protocol (Fig. 6e). Bioluminescence imaging (BLI) was used to monitor tumor establishment and growth. In the control group, bioluminescence signals appeared in the lung area around day 6, increased steadily, and migrated to the abdomen in some mice at later time points (Fig. 6g). PMEL-1 T cells alone showed no therapeutic benefit. The median survival time was 18 and 17 days, respectively, for the PBS and PMEL-1 groups (Fig. 6f). In contrast, transfer with PDCNP-Ab loaded PMEL-1 T cells significantly reduced tumor progression (Fig. 6f, g, Supplementary Fig. 32), with all animals in this group experiencing tumor regression shortly after injection (Fig. 6g). Although tumors eventually relapsed, the median survival of the animals (26 days) was significantly improved compared to the control groups.

Taken together, our results demonstrate that preloading T cells with PDCNP-Ab before adoptive cell transfer results in enhanced and more durable tumor suppression. This improvement is believed to be attributed to the ability of the nanoparticles to increase the proportion and proliferation of T_{cm} cells, which promotes prolonged persistence and overcomes the exhaustion of transferred T cells in the TME[32,33].

https://doi.org/10.1038/s41467-024-54402-y

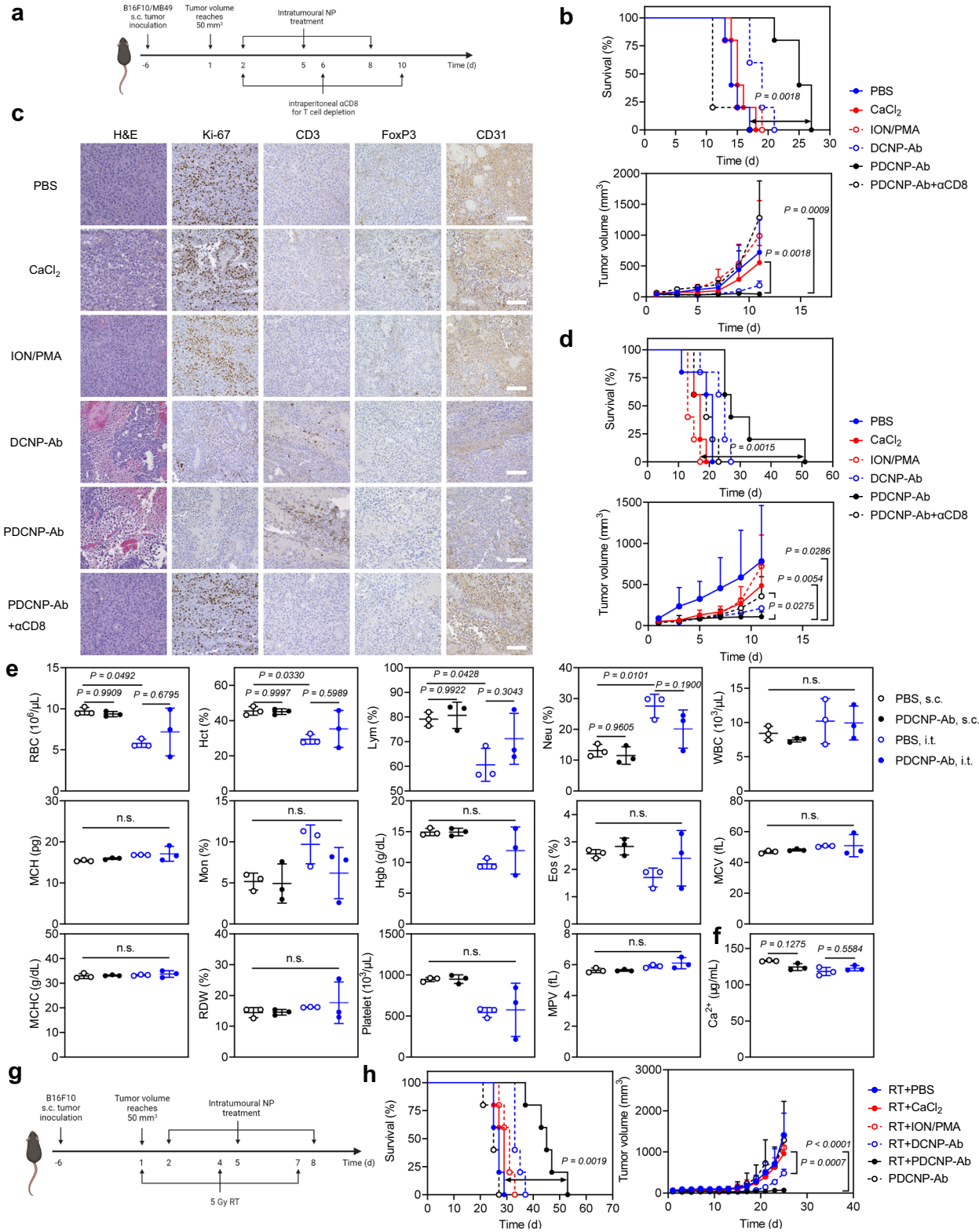

Discussion

Our research demonstrates that anti-PD-1 antibody-conjugated calcium nanoparticles can modulate cytosolic calcium levels in T cells. We showed that these nanoparticles, when loaded with PMA, can activate both endogenous CTLs and adoptively transferred T cells, resulting in enhanced tumor suppression through improved cellular immunity. PDCNP-Ab, like ION/PMA, essentially mimics the signaling pathways activated by the TCR to achieve potent CTL stimulation. Our strategy leverages calcium nanoparticles as both a calcium agent and a PMA carrier, which is proven to be effective in both in vitro and in vivo settings.

Therapies that target or harness T cells, such as immune checkpoint blockade and adoptive T cell transfer, including CAR-T, have undergone intensive investigation and achieved notable clinical success. However, challenges such as insufficient T cell proliferation and T cell exhaustion in solid tumors continue to pose significant hurdles.

Fig. 5 | Therapeutic benefit of PDCNP-Ab. PDCNP-Ab (125 μg·Ca/kg, loaded with 0.5 wt% PMA) were administered i.t. For comparison, an equivalent dose of DCNP-Ab or calcium salt was injected. **a** Timeline of nanoparticle injections. PDCNP-Ab or controls were administered i.t. on Day 2, 5, and 8. For T-cell depletion, anti-CD8 antibody (10 mg/kg) was administered i.p. on Day 2, 6, and 10. Created in BioRender. Li, J. (2024) https://BioRender.com/e46q248. Therapy studies were conducted in B16F10 tumor-bearing mice (n = 5 mice). **b** Animal survival (left) and tumor growth (right) curves. **c** Immunohistochemical analysis. Tumor specimens were stained for H&E, Ki-67, CD3, FoxP3, and CD31. Scale bars, 100 μm. **d** Animal survival (top) and tumor growth (bottom) curves. The study was performed in MB49 tumor-bearing mice (n = 5 mice). CBC (**e**) and serum calcium concentration (**f**) test results. Healthy C57BL/6 mice were injected with PBS (PBS, s.c.) or PDCNP-Ab (PDCNP-Ab, s.c.; 125 μg·Ca/kg). In addition, B16F10 tumor-bearing C57BL/6 mice injected with PBS (PBS, i.t.) or PDCNP-Ab (PDCNP-Ab, i.t.; 125 μg·Ca/kg) were tested. Animals were euthanized after 5 days, and blood samples were collected for analysis (n = 3 mice). n.s., $P > 0.05$. RBC red blood cells, Hct hematocrit, Lym lymphocytes, Neu neutrophils, WBC white blood cells, Mon monocytes, Hgb hemoglobin, Eos eosinophils, MCV mean corpuscular volume, MCH mean corpuscular hemoglobin, MCHC mean corpuscular hemoglobin concentration, RDW red cell distribution width, MPV mean platelet volume. **g** Therapeutic treatment regimen. PDCNP-Ab, DCNP-Ab, calcium salt, or ION/PMA was administered i.t. on Day 2, 5, and 8. Tumor irradiation (5 Gy) was applied on Day 1, 4, and 7. The study was conducted in B16F10 tumor-bearing mice (n = 5 mice). Created in BioRender. Li, J. (2024) https://BioRender.com/t19m381. **h** Animal survival (left) and tumor growth (right) curves. Data represent mean ± SD. Statistical difference was evaluated using an unpaired Student's t-test (one-tailed) for tumor volume in (**b, d**, and **h**); Mantel-Cox test for survival in (**b, d**, and **h**); and one-way ANOVA test in (**e**). Source data underlying (**b, d**–**f** and **h**) are provided in a Source Data file.

There is a growing need for alternative approaches that can complement existing immunotherapies. PDCNP-Ab, with fundamentally different stimulatory mechanisms, offers valuable insights into this endeavor. By bypassing upstream regulatory cues to chemically elevate $[Ca^{2+}]_i$ and activate T cells, this strategy has the potential to overcome the immunosuppressive TME and boost cellular immunity. The present study focuses on CTLs, which appear to take up more PDCNP-Ab. More studies needed to understand the effect of these nanoparticles on T helper cells and Tregs and their influence on tumor response. Future research will also develop formulations that are suitable for systemic administration or targeting other immune cells, where calcium signaling also plays a role in their activation.

Methods

Nanoparticle synthesis

Synthesis of $CaCO_3$ nanoparticles (CNP). CNPs were synthesized following a published protocol with modifications[18]. Briefly, 1359 mg of $CaCl_2$ (Sigma-Aldrich, 746495) was dissolved in 900 mL of ethanol in a 1-liter beaker. The beaker was covered with parafilm, which was then uniformly punctured with a 29G needle. The beaker was then placed inside a 3 L plastic beaker containing 36 g of NH_4HCO_3 (Sigma-Aldrich, 09830), and the entire reaction system was sealed. After approximately 60 h, nanoparticles began to form and their size was monitored by DLS. The CNPs were collected by centrifugation at 12,096 *g* for 10 min, washed with 20 mL of ethanol, and redispersed in ethanol.

Synthesis of oleic acid-coated CNPs (OCNP). Ten milligrams of CNPs dispersed in 20 mL of ethanol were mixed with 20 mg of oleic acid (Sigma-Aldrich, 364525), and the mixture was stirred overnight at room temperature. The resulting products were collected by centrifugation at 12,096 *g* for 10 min, and washed three times with a mixture of hexane/ethanol (1:2 vol/vol).

Synthesis of DSPE-PEG2000-COOH coated calcium nanoparticles (DCNP). Two milligrams of DSPE-PEG2000-COOH (Avanti Polar Lipids, 880135 P) dispersed in chloroform were mixed with 10 mg of OCNPs, and the mixture was subjected to brief sonication to obtain a homogeneous solution. Chloroform was removed with a rotary evaporator. Into the flask, 20 mL of HEPES buffer (0.01 M, pH 7.4) was added and the nanoparticles were redispersed with brief sonication. The products were collected by centrifugation at 9400 *g* for 10 min.

Synthesis of DCNP-Ab. In a typical reaction, 10 mg of DCNPs were dispersed in 2.4 mL of HEPES buffer. Into the solution, 2 mg of 1-(3-Dimethylaminopropyl)−3-ethylcarbodiimide Hydrochloride (EDC; TCI America, D1601) and 4 mg of N-hydroxysulfosuccinimide (NHS; TCI America, H1304) were added. The solution was vortexed vigorously for 20 min, and then centrifuged at 9400 *g* for 10 min. The resulting nanoparticles were redispersed in 0.75 mL of HEPES. Next, 200 μg of αPD-1 antibody (Bioxcell, BE0146) was added to the solution, which was then agitated at room temperature. If dye-labeling was desired, dye-labeled αPD-1 antibodies were used during the coupling. After 30 min, 28 μL of ethanolamine solution (Thermo scientific, 427251000; 200 mg/mL) was added and the mixture was vortexed for another 10 min to quench the reaction. The DCNP-Ab nanoparticles were collected by centrifugation at 9400 *g* for 10 min, washed for three times, redispersed in 350 μL of HEPES, and stored at 4 °C for future use. Other antibodies, including αCD3 (Bioxcell, BE0002), αCD8α (Bioxcell, BE0061), αCTLA-4 (Bioxcell, BE0164), αCD90.2 (Bioxcell, BE0066), and mouse IgG (Invitrogen, 31903), were conjugated following the same protocol.

Synthesis of PDCNP-Ab. DCNP-Ab with a desired calcium concentration were dispersed in HEPES. PMA (Sigma-Aldrich, P8139; 10 μg/mL, in acetonitrile) was added into the solution, which was then sonicated for 1 min to facilitate the loading process. The products were collected centrifugation.

Nanoparticle characterization

Nanoparticle size and morphology were characterized by TEM and scanning electron microscopy (SEM) using a STEM-Hitachi SU9000EA instrument operated at 30 kV and 2 μA. Nanoparticle size distributions in the microscopic images were analyzed using ImageJ software. EDX spectra were obtained using the STEM-Hitachi SU9000EA system and the FEI Teneo machine. The crystallinity of the nanoparticles was evaluated using a Bruker D8-Advance X-ray diffraction instrument. FT-IR spectra were recorded on a Nicolet iS10 FT-IR spectrometer. The hydrodynamic sizes and zeta potentials of the nanoparticles were measured using a Malvern Zetasizer Nano ZS system. To quantify the calcium content in the nanoparticles, 20 μL nanoparticle solution was mixed with 80 μL 5% HNO_3 solution and sonicated for 1 h followed by overnight incubation. The concentration was then measured using a colorimetric calcium assay kit (Abcam, ab102505) according to the manufacturer's protocol.

The antibody conjugation valency was calculated using the following equation:

$$\text{Valency of conjugated antibody} = \frac{\frac{CaCO3\ mass}{CaCO3\ NP\ mass}}{mole\ of\ antibody} \quad (1)$$

The mass of a single $CaCO_3$ nanoparticle was estimated using the following equation:

$$CaCO_3\text{NP mass} = \frac{4}{3}\pi r^3 \times CaCO_3\text{density} \times 6.022 \times 10^{23} = 1.14 \times 10^9 \text{g/mol} \quad (2)$$

To quantify the amount of PMA incorporated into PDCNP-Ab, the nanoparticles were dispersed in acetonitrile, followed by sonication for 1 h. After resting overnight, the PMA content was measured by HPLC using an LC-20AR HPLC system (Shimadzu, Japan) equipped with a UV detector SPD-20A, an autosampler SIL-20AHT, and an Inertsil ODS-4 analytical column (5 μm, 4.6 mm × 250 mm, GL Sciences). The

https://doi.org/10.1038/s41467-024-54402-y

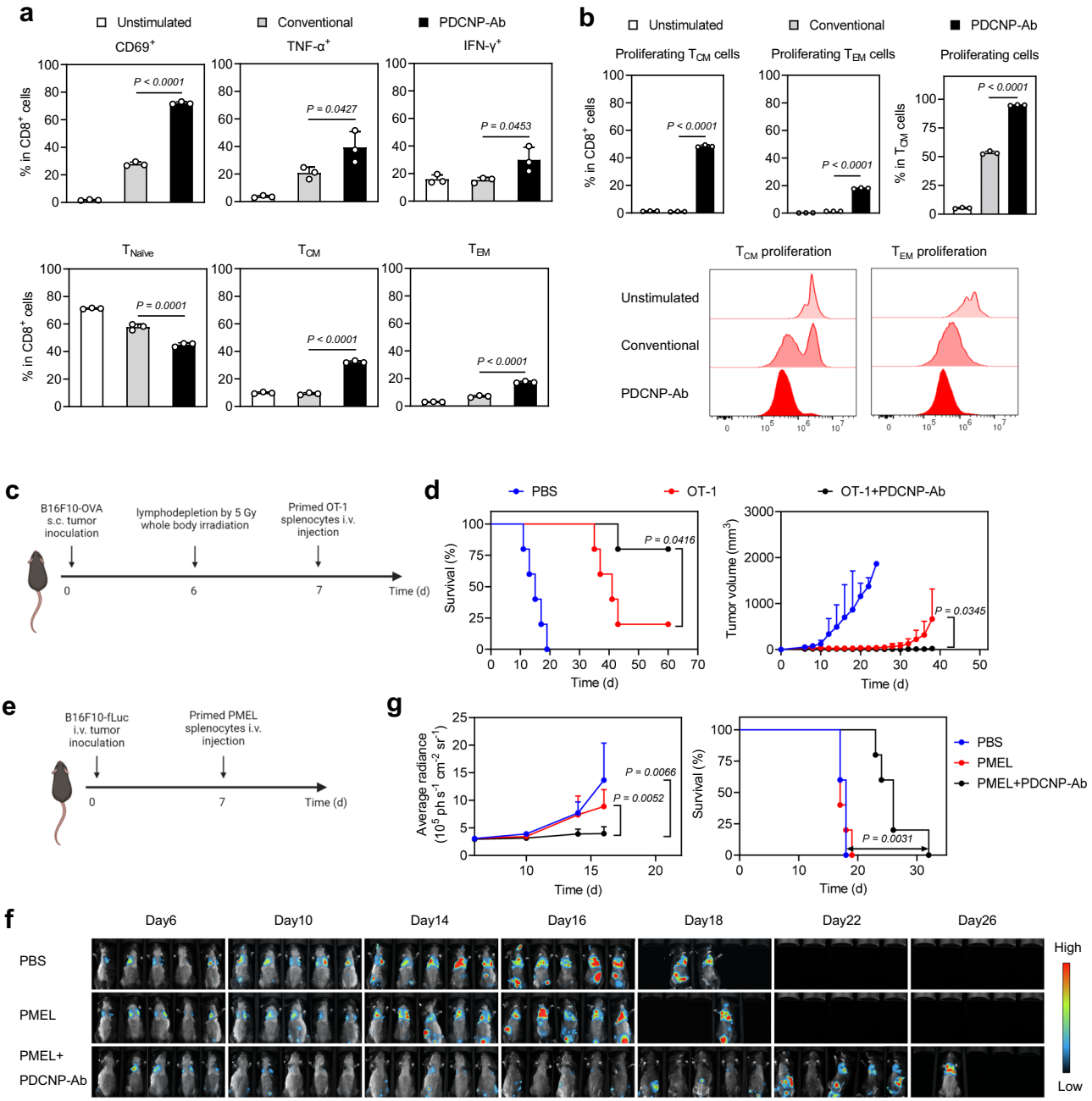

Fig. 6 | Effect of PDCNP-Ab on adoptive cell therapy. Analysis of OT-1 splenocytes after treatment with a conventional protocol or PDCNP-Ab (n = 3 biologically independent samples). **a** Analysis of T-cell activation markers, including CD69, TNF-α, and IFN-γ, and memory T cell phenotypes. **b** Analysis of T-cell proliferation and differentiation into T_{CM} or T_{EM}. **c** Scheme of testing adoptive cell therapy with PDCNP-Ab loaded OT-1 cells in mice bearing flank B16F10-OVA tumors. PBS or OT-1 splenocytes (8×10^6/mouse), activated with either a conventional protocol or with PDCNP-Ab, were fused i.v. into animals 7 days after tumor inoculation (n = 5 mice). Created in BioRender. Li, J. (2024) https://BioRender.com/j90x668. **d** Animal survival (left) and tumor growth curves (right). **e** Scheme of testing adoptive cell therapy with PDCNP-Ab-loaded PMEL-1 T cells. The study was conducted in a metastatic tumor model established with i.v. administered B16F10-fluc cells. PBS or splenocytes from PMEL-1 mice (8×10^6/mouse), activated with either a conventional protocol or with PDCNP-Ab, were fused i.v. into animals 7 days after tumor inoculation (n = 5 mice). Created in BioRender. Li, J. (2024) https://BioRender.com/d83g701. **f** Whole-body bioluminescence images taken at different time points to monitor tumor establishment and metastasis. **g** Left, tumor growth curves, based on region-of-interest (ROI) analysis of BLI images; right, animal survival curves. Data represent mean ± SD. Statistical difference was evaluated using a one-way ANOVA test in (**a**–**b**); Mantel-Cox test in (**d**, **g**) (survival); and unpaired t-test (one-tailed) in (**d, g**) (tumor volume). Source data underlying (**a**–**b, d** and **g**) are provided in a Source Data file.

analysis employed a mobile phase consisting of 0.1% trifluoroacetic acid in water (A) and 0.1% trifluoroacetic acid in acetonitrile (B), with an isocratic elution of 90% B at a flow rate of 1.0 mL/min over a 40-min run time. The UV detector was set at 280 nm, and the analysis was performed at 40 °C.

Cell culture

Mouse T-lymphoblast cell line EL4 and mouse melanoma cell line B16F10 were obtained from the American Type Culture Collection (ATCC). B16F10-OVA and B16F10-fLuc cell lines were a kind gift from Dr. Houjian Cai of University of Georgia. EL4 cells were maintained in

Dulbecco's minimum essential medium (DMEM, ATCC, 30-2002) supplemented with supplemented with 10% horse serum (Invitrogen, 00-4970-93) and 1% penicillin-streptomycin (Gibco, 15140-122). B16F10 and B16F10-fLuc cells were cultured in DMEM medium supplemented with 10% fetal bovine serum (FBS; R&D, S11150H) and 1% penicillin-streptomycin. B16F10-OVA cells were maintained in complete DMEM medium supplemented with 0.5 mg/mL G418 sulfate (Gibco, 10131027).

Splenocytes were isolated from spleens from C57BL/6, OT-1, or PMEL-1 mice. Spleen tissue was passed through a 70 μm cell strainer (Corning Falcon, 352235). Cells were centrifuged at 600 *g* for 6 min and washed twice with cold PBS. Splenocytes were cultured in RPMI 1640 medium (Corning, 10-040-CV) supplemented with 10% FBS, 1% penicillin-streptomycin, 1% HEPES buffer, and 0.4% mercaptoethanol.

Human CD3 Pan T cells (Biosciences, IQB-Hu1-T10, Donor ID 0058) were thawed and activated with Dynabeads (Thermo Scientific, 11161D) at a 1:1 ratio, and cultured in TexMACS medium (Miltenyi, 130-097-196) supplemented with IL-2 (40 U/mL) for 4 days. Beads were then removed, and the cells were cultured until Day 10 for use in experiments.

All cells were maintained in a humidified 37 °C incubator with a 5% carbon dioxide atmosphere.

T cell isolation and priming

Spleens from C57BL/6 or OT-1 mice were processed through a 70 μm cell strainer (Corning Falcon, 352235) to obtain a single-cell suspension, which was then washed with PBS. Naïve splenocytes were used directly. To generate primed $CD8^+$ OT-1 T cells, splenocytes were cultured with αCD3 (Invitrogen, 16003185)/αCD28 (Invitrogen, 16028185) at a concentration of 0.3 mg/mL or incubated with OVA 257-264 peptide (SIINFEKL; InvivoGen, vac-sin) at a concentration of 10 ng/mL. For $CD8^+$ OT-1 T cell enrichment, naïve splenocytes were treated with OVA peptide (10 ng/mL) and recombinant mouse IL-2 (10 ng/mL; Biolegend, 575406) for 2 days. $CD8^+$ T cells were then enriched using the EasySep kit (Stemcell, 19853). The cells were resuspended in a medium containing IL-2 (10 ng/mL) at 1.5 M/mL and collected after 24 h for further use.

Cell studies

Binding avidity. To assess cell binding avidity, EL4 or OT-1 T cells were fixed with a mixture of IC fixation buffer (eBioscience, 00-8222-49) and staining buffer (eBioscience, 00-4222-57) for 20 min, and then resuspended in blocking buffer (PBS with 5% BSA, Sigma-Aldrich, A2153) to block nonspecific interactions. Cy5-labeled nanoparticles were incubated with the cell suspension for 2 h and washed three times with 5% PBS-BSA buffer before analysis by flow cytometry.

Cellular uptake. T cells or splenocytes were seeded in a 6-well plate at a density of 1 million cells per well. Cy5-labeled nanoparticles were incubated with the cells for 24 h, and washed with PBS. Prior to flow cytometry analysis, trypan blue (20 μg/mL) was incubated with the cells in the dark for 5 min to quench the signals from surface-bound nanoparticles. For comparison, the incubation was performed at 4 °C or in the presence of endocytosis inhibitors such as Dynasore (80 μM, Sigma, D7693) or Nystatin (25 μM, Sigma, N6261).

Intracellular calcium concentration. Cellular $[Ca^{2+}]_i$ was probed using Fluo-3 AM (Cayman, 14960) according to the protocol provided by the vendor. Cells were seeded in a 6-well plate at a density of 1 million cells per well and were incubated with DCNP-Ab (10 μg·Ca/mL). For time-dependent studies, Fluo-3 intensity was measured at different time points using a microplate reader (Synergy Mx, BioTeK). Alternatively, cells were collected after 24 h and analyzed by flow cytometry (NovoCyte Quanteon, Agilent).

Cytotoxicity. The toxicity of nanoparticles to T cells was measured by either ATP luminescence assay (PerkinElmer, 6016736) following the manufacture's protocol or by standard MTT (Sigma-Aldrich, M2128) assay.

Western blotting

After incubation with PBS, ION/PMA, DCNP-Ab, or PDCNP-Ab for 24 h, cells were then lysed with RIPA buffer (Thermo Scientific, 89901) supplemented with 100× HaltTM Proteinase and Phosphatase Inhibitor Cocktail (Thermo Scientific, 78445). Protein concentration in cell lysates was measured using a DC protein assay kit (BioRad). Protein lysates were loaded onto a 10% SDS-PAGE gel and transferred to PVDF membranes. To block nonspecific binding, membranes were incubated with 5% bovine serum albumin (BSA, Sigma-Aldrich) for 1 h at room temperature. Membranes were then incubated with primary antibodies overnight at 4 °C with gentle shaking. After washing, membranes were incubated with secondary antibodies for 1 h at room temperature. Membranes were incubated with Clarity Max Western ECL Substrate (BioRad, 1705062) and exposed to X-ray films for signal detection. Equal protein loading was confirmed by probing for GAPDH. Antibodies used for detection were: NF-κB (Cell Signaling, 8242T, 1:1000), p-NF-κB (Cell Signaling, 3033T, 1:1000), IκBα (Cell Signaling, 4814T, 1:1000), p-IκBα (Cell Signaling, 2859 T, 1:1000), NFAT (Cell Signaling, 4389S, 1:1000), p-NFAT (Abcam, ab200819, 1:1000), and GAPDH (Cell Signaling, 2118L, 1:1000).

Mice

All animal experimental procedures were conducted following protocols approved by the Institutional Animal Care and Use Committee (IACUC) of the University of Georgia, and were carried out in accordance with the relevant guidelines and regulations and also reported in accordance with ARRIVE guidelines. Female C57BL/6 mice (4–5 weeks old, stock# 044) and nude mice (4–5 weeks old, stock# 6902) were procured from Envigo. TCR transgenic mice, including OT-1 (C57BL/6-Tg(TcraTcrb)1100Mjb/J, stock# 003831) and PMEL-1 (B6.Cg-Thy1a/Cy Tg(TcraTcrb)8Rest/J, stock# 005023) mice, were obtained from the Jackson Laboratory (4–5 weeks old). All mice were housed in a pathogen-free environment in 12-h light-dark cycle, at 22 °C and 30% relative humidity. Mice were euthanized by cervical dislocation under deep anesthesia.

Cytokine measurement

To measure cytokines in the cell culture supernatant, cells were centrifuged, and the supernatant was collected and diluted by ×2, ×10, or ×50. To measure cytokines in the TME, tumor samples were homogenized in Hank's Balanced Salt Solution (HBSS, Gibco, 14175-079) with a tumor concentration of 100 mg/mL supplemented with proteinase and phosphatase inhibitors. The homogenized samples were then subjected to centrifugation at 10,000 *g* for 15 min to separate the supernatant containing the cellular components from any remaining cellular debris. Total protein levels in the supernatant were quantified using a DC protein assay kit. Targeted cytokine levels were measured using ELISA kits according to the vendor's protocol. The ELISA kits used were IL-2 (R&D, DY402), TNF-α (R&D, DY410), IFN-γ (R&D, DY485), and IL-10 (R&D, DY417).

Flow cytometry

Tumor tissues were cut into small pieces and digested with a mixture of DMEM supplemented with 1 mg/mL collagenase type V (Sigma-Aldrich, C6885), 1x GlutaMax (Gibco, 35050061), and 100 U/mL DNase I (Invitrogen, 18047019) at 37 °C for 50 min. The digested tissue was then meshed through a 250 μm tissue strainer (Pierce, 87791) to obtain single-cell suspension. TDLN and spleen samples were processed using the same method as for T cell isolation. The resulting single cell suspension was washed with cold PBS and dispersed in staining buffer for

antibody staining. For ex vivo analysis, splenocytes were co-cultured with B16F10-OVA cancer cells at a ratio of 5:1 in DMEM supplemented with monensin (Invitrogen, 00-4505-51) for 4 h.

For staining, collected cells were first treated with CD16/32 antibody (Biolegend, 101320; 1:1000 dilution) to block Fc receptor-mediated nonspecific binding. For staining of intracellular markers, GolgiPlug (BD, 555029) was added to the cell culture medium 4 h before cell collection. Following the blocking step, the cells were stained with antibodies specific for their respective targets 30 min. After staining, the cells were fixed with an IC fixation buffer for a period of 20 min. Permeabilization buffer (Invitrogen, 00833356) was used to dilute intracellular antibody markers and stain the cells for 30 min. The stained cells were analyzed by flow cytometry on an Agilent NovoCyte Quanteon system according to the manufacturer's instructions. AbC total antibody compensation bead kit (Invitrogen, A10497) was used for compensation. Fluorescence-labeled antibodies used in this study include CD45 (BD, 557659, 1:80), CD8 (Biolegend, 100752, 1:80), CD4 (Biolegend, 100451, 1:80), CD3 (Biolegend, 100210, 1:50), FoxP3 (Biolegend, 126404, 1:20), CD25 (Biolegend, 101918, 1:33), T-bet (Biolegend, 644814, 1:40), GATA3 (Biolegend, 653814, 1:20), IFN-γ (Biolegend, 505808, 1:20), TNF-α (Biolegend, 506306, 1:20), CD11c (Biolegend, 117343, 1:20), CD11b (Biolegend, 101206, 1:67), CD19 (Biolegend, 152412, 1:40), CD69 (Biolegend, 104530, 1:33), CD44 (Biolegend, 103008, 1:40), CD62L (Biolegend, 104412, 1:40), PD-1 (eBioscience, 46998182, 1:67), EOMES (eBioscience, 12487582, 1:20), Ki-67 (Invitrogen, 46569882, 1:50), TIM3 (Biolegend, 134019, 1:40), LAG3 (eBioscience, 47223182, 1:20), and anti-human CD8 (Biolegend, 303804, 1:20). Specific cell populations were defined as follows: CTLs ($CD8^+$), effector CTLs ($CD8^+IFN\text{-}\gamma^+$), Tregs ($CD4^+CD25^+FoxP3^+$), Th1 ($CD4^+T\text{-}bet^+$), Th2 ($CD4^+GATA3^+$), DCs ($CD11c^+$), macrophages ($CD11b^+$), B cells ($CD19^+$), T_{EM} ($CD44^+CD62L^-$), and T_{CM} ($CD44^+CD62L^+$). The gating strategies are described in Supplementary Figs. 33–35.

Nanoparticle retention in tumor and intratumoral distribution

Nanoparticle retention in tumors was evaluated in MB49-bearing C57BL/6 mice. When tumor size reached 300 mm^3, Cy5.5-labeled DCNP or DCNP-Ab (1 nmol/kg, based on dye concentration) were injected i.t. Whole-body fluorescence images were acquired on a NEWTON 7.0 Bio system at 1, 2, 4, 8, 12, and 24 h post-injection. Mice were euthanized after the 24-h scan. Major organs were subjected to ex vivo imaging. Tumor samples were snap-frozen in O.C.T. and sectioned into 4-µm thick slices for microscopic imaging on a Keyence BZ-X810 system.

The intratumoral tumor distribution of the nanoparticles was further evaluated in B16F10-bearing C57BL/6 mice. When the tumor size reached 300 mm^3, radiation was applied to the tumor at a dose of 5 Gy, followed by the injection of Cy5-labeled nanoparticles one day later. After another 24 h, the animals were euthanized. The tumor tissues were processed into single cells for flow cytometry analysis.

Safety-related studies

The potential toxicity of the nanoparticles was evaluated in B16F10-bearing C57BL/6 mice. When the tumor size reached 50 mm^3, the animals received three doses of intratumoral PBS or PDCNP-Ab (125 µg calcium per kg) 3 days apart. In addition, healthy mice receiving subcutaneous injection of PBS or PDCNP-Ab were also tested. All animals were euthanized 5 days after the last injection. Fresh blood samples were collected for CBC and biochemical analyses. Serum was obtained by centrifugation of coagulated blood at 1500 *g* for 15 min. Serum calcium level was measured using a colorimetric calcium assay kit (Abcam, ab102505) following the vendor's protocol. Major organ tissues were harvested and fixed in formalin. CBC, biochemistry, and histopathology were performed in the Histology Laboratory, at the Department of Pathology, UGA College of Veterinary Medicine.

Therapeutic efficacy

The therapeutic benefit of intratumoral PDCNP-Ab was evaluated in subcutaneous tumor models established in C57BL/6 mice. Briefly, B16F10, B16F10-OVA, or MB49 cancer cells were injected subcutaneously at a concentration of 0.5×10^6 cells in a mixture of 25 µL cell culture medium and 25 µL matrigel (Corning, 354234). Tumor size was measured every two days with a caliper, and mouse body weight was monitored throughout the experiment. Tumor volume was calculated using the equation: tumor volume = (length) × $(width)^2/2$. Treatment started when tumor size reached ~50 mm^3 (Day 1). For CTL depletion, αCD8 antibodies (Bioxcell, BE0004) were injected intraperitoneally at a dose of 10 mg/kg on Day 2, 6, and 10. For irradiation-related studies, irradiation was administered using an X-RAD system. Animals were euthanized when the tumor masses reached 1.7 cm in one dimension or exhibited severe weight loss or tumor ulceration. Tumor tissues were sectioned into 4-µm-thick slices and stained for H&E, Ki-67, CD3, FoxP3, and CD31.

The influence of PDCNP-Ab on adoptive cell therapy was evaluated in both subcutaneous and metastatic tumor models. The establishment of subcutaneous tumor model was the same as described above. Lymphodepletion was performed by irradiation (5 Gy) of the whole animal body except for the tumor area 6 days after tumor inoculation. OT-1 splenocytes were collected from OT-1 mice as described above and activated by incubation with OVA peptide (10 ng/mL) and mouse IL-2 (10 ng/mL) for 5 days. PDCNP-Ab (10 µg·Ca/mL, 0.5 wt% PMA) was then substituted for OVA peptide in the PDCNP-Ab group and was incubated with the cells for 24 h. After 24 h, the splenocytes were collected and intravenously infused into tumor-bearing mice at a dose of 8×10^6 cells per mouse.

The metastatic tumor model was established by i.v. injection of 0.5×10^6 B16F10-fLuc cells into C57BL/6 mice on Day 0. PMEL-1 splenocytes were collected from PMEL-1 mice as previously described and activated by incubation with mouse gp100 peptide (10 µg/mL, AnaSpec, AS-64752) and mouse IL-2 (10 ng/mL) for 5 days. PDCNP-Ab (10 µg·Ca/mL, 0.5 wt% PMA) then replaced the peptide antigen in the PDCNP-Ab group to incubate with the cells. After 24 h, the splenocytes were collected and intravenously infused into tumor-bearing mice at a dose of 8×10^6 cells per mouse. For bioluminescence imaging, 150 mg/kg of luciferin (Goldbio, LUCK) was injected intraperitoneally, and whole-body images were acquired using a NEWTON 7.0 Biosystem.

Immunohistochemical analyses

Tumor samples collected from mice were embedded in O.C.T. compound (Sakura Finetek, 4583) and frozen at −80 °C. Tissue sections of 6-µm thickness were prepared and were fixed in cold acetone for 10 min at 4 °C. Slides were then washed, blocked with a 5% BSA-PBS solution, and stained with primary antibodies, including anti-CD8 (Invitrogen, MA5-29682, 1:100) and anti-PD-1 (Bioxcell, BE0273, 1:100) antibodies, overnight at 4 °C. After washing, secondary antibodies, including goat anti-rabbit AF488 (Invitrogen, A-11008, 1:500) and goat anti-rat AF555 (Invitrogen, A-21434, 1:200), were added and incubated with the slides for 2 h in the dark. The slides were then mounted with mounting medium containing with DAPI (Vectashield, H-1200). Microscopic imaging was performed on a Keyence BZ-X810 system.

Statistical analysis

All measurements in our study were performed with at least three biological replicates, unless otherwise noted. Data are presented as means with error bars representing the standard deviation. Statistical comparisons between multiple assays were performed using one-way analysis of variance (ANOVA). Unpaired Student's *t*-tests were used for comparisons between two groups. A *p*-value less than 0.05 was considered statistically significant. All statistical analyses were performed with GraphPad Prism 9 software.

Reporting summary
Further information on research design is available in the Nature Portfolio Reporting Summary linked to this article.

Data availability
The main data supporting the results of this study are available within the paper and its Supplementary Information. All data generated in this study are available from the corresponding authors upon reasonable request. Source data are provided with this paper.

References

1. Martínez-Lostao, L., Anel, A. & Pardo, J. How do cytotoxic lymphocytes kill cancer cells? *Clin. Cancer Res.* **21**, 5047–5056 (2015).
2. Barry, M. & Bleackley, R. C. Cytotoxic T lymphocytes: all roads lead to death. *Nat. Rev. Immunol.* **2**, 401–409 (2002).
3. Golstein, P. & Griffiths, G. M. An early history of T cell-mediated cytotoxicity. *Nat. Rev. Immunol.* **18**, 527–535 (2018).
4. Philip, M. & Schietinger, A. CD8+ T cell differentiation and dysfunction in cancer. *Nat. Rev. Immunol.* **22**, 209–223 (2022).
5. Chow, A., Perica, K., Klebanoff, C. A. & Wolchok, J. D. Clinical implications of T cell exhaustion for cancer immunotherapy. *Nat. Rev. Clin. Oncol.* **19**, 775–790 (2022).
6. Arner E. N., Rathmell J. C. Metabolic programming and immune suppression in the tumor microenvironment. *Cancer Cell* 2023.
7. Postow, M. A., Callahan, M. K. & Wolchok, J. D. Immune checkpoint blockade in cancer therapy. *J. Clin. Oncol.* **33**, 1974 (2015).
8. de Coaña, Y. P., Choudhury, A. & Kiessling, R. Checkpoint blockade for cancer therapy: revitalizing a suppressed immune system. *Trends Mol. Med.* **21**, 482–491 (2015).
9. Topalian, S. L., Taube, J. M., Anders, R. A. & Pardoll, D. M. Mechanism-driven biomarkers to guide immune checkpoint blockade in cancer therapy. *Nat. Rev. Cancer* **16**, 275–287 (2016).
10. Yarchoan, M., Hopkins, A. & Jaffee, E. M. Tumor mutational burden and response rate to PD-1 inhibition. *N. Engl. J. Med.* **377**, 2500–2501 (2017).
11. Sharma, P., Hu-Lieskovan, S., Wargo, J. A. & Ribas, A. Primary, adaptive, and acquired resistance to cancer immunotherapy. *Cell* **168**, 707–723 (2017).
12. Schwarz, E. C., Qu, B. & Hoth, M. Calcium, cancer and killing: the role of calcium in killing cancer cells by cytotoxic T lymphocytes and natural killer cells. *Biochim. Biophys. Acta (BBA)-Mol. Cell Res.* **1833**, 1603–1611 (2013).
13. Trebak, M. & Kinet, J.-P. Calcium signalling in T cells. *Nat. Rev. Immunol.* **19**, 154–169 (2019).
14. Lewis, R. S. Calcium signaling mechanisms in T lymphocytes. *Annu. Rev. Immunol.* **19**, 497–521 (2001).
15. Toldi G. The regulation of calcium homeostasis in T lymphocytes. *Front. Immunol.* **4**, 432 (2013).
16. Vaeth, M., Kahlfuss, S. & Feske, S. CRAC channels and calcium signaling in T cell-mediated immunity. *Trends Immunol.* **41**, 878–901 (2020).
17. Chatila, T., Silverman, L., Miller, R. & Geha, R. Mechanisms of T cell activation by the calcium ionophore ionomycin. *J. Immunol.* **143**, 1283–1289 (1989).
18. Kim, J. et al. Improved suspension stability of calcium carbonate nanoparticles by surface modification with oleic acid and phospholipid. *Biotechnol. Bioprocess Eng.* **20**, 794–799 (2015).
19. Shumilina, E., Huber, S. M. & Lang, F. Ca2+ signaling in the regulation of dendritic cell functions. *Am. J. Physiol.-Cell Physiol.* **300**, C1205–C1214 (2011).
20. Gros, A. et al. PD-1 identifies the patient-specific CD8+ tumor-reactive repertoire infiltrating human tumors. *J. Clin. Investig.* **124**, 2246–2259 (2014).
21. Zhang, H. et al. Regulatory mechanisms of immune checkpoints PD-L1 and CTLA-4 in cancer. *J. Exp. Clin. Cancer Res.* **40**, 1–22 (2021).
22. Rennick, J. J., Johnston, A. P. & Parton, R. G. Key principles and methods for studying the endocytosis of biological and nanoparticle therapeutics. *Nat. Nanotechnol.* **16**, 266–276 (2021).
23. Bell, J. T-cell turn-off. *Nat. Rev. Immunol.* **2**, 460–460 (2002).
24. Kumar, A., Moreau, J.-L., Gibert, M. & Thèze, J. Internalization of interleukin 2 (IL-2) by high affinity IL-2 receptors is required for the growth of IL-2-dependent T cell lines. *J. Immunol.* **139**, 3680–3684 (1987).
25. Fujii, M. et al. High-affinity receptor-mediated internalization and degradation of interleukin 2 in human T cells. *J. Exp. Med.* **163**, 550–562 (1986).
26. Campbell, D. J. & Koch, M. A. Phenotypical and functional specialization of FOXP3+ regulatory T cells. *Nat. Rev. Immunol.* **11**, 119–130 (2011).
27. Boissonnas, A. et al. Foxp3+ T cells induce perforin-dependent dendritic cell death in tumor-draining lymph nodes. *Immunity* **32**, 266–278 (2010).
28. McLane, L. M. et al. Role of nuclear localization in the regulation and function of T-bet and Eomes in exhausted CD8 T cells. *Cell Rep.* **35**(6) (2021).
29. Wen, L. et al. The research progress of PD-1/PD-L1 inhibitors enhancing radiotherapy efficacy. *Front. Oncol.* **11**, 799957 (2021).
30. Trappetti, V. et al. Microbeam radiation therapy controls local growth of radioresistant melanoma and treats out-of-field locoregional metastasis. *Int. J. Radiat. Oncol.* Biol.* Phys.* **114**, 478–493 (2022).
31. Vodnala, S. K. et al. T cell stemness and dysfunction in tumors are triggered by a common mechanism. *Science* **363**, eaau0135 (2019).
32. Gattinoni, L., Speiser, D. E., Lichterfeld, M. & Bonini, C. T memory stem cells in health and disease. *Nat. Med.* **23**, 18–27 (2017).
33. Kim, M. Y. et al. A long-acting interleukin-7, rhIL-7-hyFc, enhances CAR T cell expansion, persistence, and anti-tumor activity. *Nat. Commun.* **13**, 3296 (2022).

Acknowledgements
This research received support from the National Cancer Institute (grant nos. R01CA247769 & R01CA257851 to J.X.), the Department of Defense Congressionally Directed Medical Research Programs (HT94252410734 to J.X.), the National Institute of Dental and Craniofacial Research (R01DE028351 to Y.T.), and the National Institute of General Medical Sciences (R35GM143067 to Y.L.). We also thank support from the Developmental Funds from Winship Cancer Institute of Emory University and the University of Georgia (to Y.T. and J.X.) under award number P30CA138292, the Georgia Center for Oncology Research and Education (Georgia CORE, to J.X. and Y.T.), and the Georgia Regenerative Engineering and Medicine Center (to J.X. and Y.T.).

Author contributions
W.Y. and J.X. conceived the study and designed the experiments. Y.T., G.Z., and W.T.W. contributed to immune-related experiment design and data interpretation. W.Y., Z.C., Z.F., J.L., F.J., F.C., S.Z., F.K., and X.L. performed the experiments and generated the data. L.Y., Y.T., W.Y., G.Z., and J.X. analyzed the data and summarized the paper.

Competing interests
The University of Georgia has filed a patent application on the technology and intellectual property reported here for which W.Y., Z.C., and J.X. are inventors. The remaining authors declare no competing interests.

Additional information

Supplementary information The online version contains supplementary material available at https://doi.org/10.1038/s41467-024-54402-y.

Correspondence and requests for materials should be addressed to Gang Zhou or Jin Xie.

Peer review information *Nature Communications* thanks the anonymous reviewer(s) for their contribution to the peer review of this work. A peer review file is available.